Al 3p occupied states in Al-Cu-Fe intermetallics and enhanced stability of the icosahedral quasicrystal

2000 J. Phys.: Condens. Matter 12 8159

(http://iopscience.iop.org/0953-8984/12/37/314)

J. Phys.: Condens. Matter **12** (2000) 8159–8177. Printed in the UK PII: S0953-8984(00)12087-9

Al 3p occupied states in Al–Cu–Fe intermetallics and enhanced stability of the icosahedral quasicrystal

Esther Belin-Ferré†§, Vincent Fournée† and Jean Marie Dubois‡

† Laboratoire de Chimie Physique Matière et Rayonnement, Unité Mixte de Recherche 7614 and Groupement de Recherche Concertation pour l'Investigation des Quasicristaux, 11 rue Pierre et Marie Curie, F-75231 Paris Cédex 05, France

‡ Laboratoire de Science et Génie des Matériaux Métalliques, Unité Mixte de Recherche 7584 and Groupement de Recherche Concertation pour l'Investigation des Quasicristaux, Centre d'Ingénierie des Matériaux, Ecole des Mines, Parc de Saurupt, F-54042 Nancy Cédex, France

E-mail: belin@ccr.jussieu.fr

Received 24 February 2000, in final form 13 June 2000

Abstract. This paper concentrates on a comparison of Al 3p occupied densities of states in crystalline and quasicrystalline Al–Cu–Fe intermetallics. This comparison is made quantitative by computing the two first moments of this partial distribution, which correspond to the partial contribution of Al atoms to the cohesive energy of the material and to the orbital overlap modulated by the coordination number, respectively. From these data, we conclude that the icosahedral quasicrystal and its approximants represent a region of specifically enhanced stability in the Al–Cu–Fe phase diagram. We assign this effect to the specific role played by Al 3p states in the Hume-Rothery mechanism. We confirm the occurrence of a stronger hybridization between Al 3p and Fe 3d states in the icosahedral structure whereas we point out a weaker interaction with Cu 3d states in the icosahedral compounds as compared to stable approximants.

1. Introduction

The clearest evidence that icosahedral quasicrystals can no longer be considered as artefacts of crystalline order is supported by the existence of series of crystalline approximants with huge unit cells and large lattice parameters ranging between 1.2 and 12 nm. Such approximants have been found so far in a variety of systems. They show diffraction patterns resembling but also clearly distinct from those of true quasicrystals. For instance, in the Al–Cu–Fe system have been discovered approximants with rhombohedral, orthorhombic and pentagonal structures (Audier and Guyot 1989, Calvayrac *et al* 1990, Gratias *et al* 1993, Quiquandon *et al* 1995). Quiquandon *et al* (1996) and Quivy *et al* (1996) reported also the existence of a so-called 1/1 cubic approximant of nominal composition $Al_{55}Si_7Cu_{25.5}Fe_{12.5}$. Quiquandon *et al* (1999) mentioned later that minute changes of composition in this system lead to the existence of two kinds of cubic approximant based respectively on the Mackay and Bergman polyhedral clusters.

It is commonly accepted that the knowledge of the properties of approximants, especially when going closer and closer to the quasicrystalline compound, may give insight into the intrinsic properties of the quasicrystal. So far, the electronic properties and local structure of many of the Al–Cu–Fe approximants have been investigated by various techniques such

§ Contact author.

0953-8984/00/378159+19$30.00

Table 1. List of the samples, their composition, crystallographic structure and parameters, electron per atom ratio and symbols used in the figures.

Sample	Formula	Structure	Lattice parameters	e/a (e^-/at)	Symbol used in figures
Free-electron metal	Al	fcc	$a = 0.404$ nm	3.0	??
Hume-Rothery crystals	γ-$Al_{35}Cu_{65}$	cubic	$a = 0.8703$ nm	1.7	♦
	δ-$Al_{39}Cu_{61}$	rhombohedral	$a = 0.8789$ nm $\alpha = 89.73^\circ$	1.78	♦
	ξ-$Al_{43}Cu_{57}$	monoclinic	$a = 0.707$ nm $b = 0.408$ nm $c = 1.002$ nm $\beta = 90.63^\circ$	1.86	♦
	η-$Al_{50}Cu_{50}$	monoclinic	$a = 1.2066$ nm $b = 0.4105$ nm $c = 0.691$ nm $\beta = 124.96^\circ$	2.0	♦
	θ-Al_2Cu	tetragonal	$a = 0.64$ nm $c = 0.486$ nm	2.33	♦
	ϕ-$Al_{10}Cu_{10}Fe$	hexagonal	$a = 0.4106$ nm $c = 0.5095$ nm	1.81	◇
	ω-Al_7Cu_2Fe	tetragonal	$a = 0.633$ nm $c = 1.481$ nm	2.1	○
β-phases	$Al_{46}Cu_{36}Fe_{18}$	cubic, CsCl type		1.38	□
	$Al_{50}Cu_{35}Fe_{15}$	cubic, CsCl type		1.55	□
	$Al_{55}Cu_{33}Fe_{12}$	cubic, CsCl type		1.74	□
Approximants	$Al_{60.7}Cu_{29.5}Fe_{19.8}$	orthorhombic	$a = 3.216$ nm $b = 11.63$ nm $c = 1.985$ nm	1.72	■
	$Al_{62.5}Cu_{25.5}Fe_{11}$	rhombohedral	$a = 3.214$ nm $\beta = 36^\circ$	1.88	■
	$Al_{63.6}Cu_{24.5}Fe_{11.9}$	pentagonal	5.231 nm (periodic axis)	1.915	■
	$Al_{55}Si_7Cu_{25.5}Fe_{12}$	1/1 cubic	$a = 1.24$ nm	1.945	■
	$Al_{62.8}Cu_{26}Fe_{11.2}$	rhombohedral		1.92	
	$Al_{61.8}Cu_{28}Fe_{10.4}$	rhombohedral		1.926	
Quasicrystals	$Al_{62}Cu_{25.5}Fe_{12.5}$	perfect icosahedral		1.865	●
	$Al_{70.5}Pd_{21}Mn_{8.5}$	icosahedral		1.86	○
	$Al_{62.8}Cu_{26}Fe_{11.2}$	icosahedral		1.92	
	$Al_{61.8}Cu_{28}Fe_{10.4}$	icosahedral		1.926	

as resistivity measurements (Berger 1994 and references therein, Berger *et al* 1995, Quivy *et al* 1996), nuclear magnetic resonance (Hippert *et al* 1995, Hippert 1997), EXAFS (Sadoc *et al* 1993a) and electron and x-ray diffraction measurements, applied to single crystals when available (Kang *et al* 1992, Sugiyama *et al* 1998, Yamada *et al* 1999). On the other hand, calculations of the densities of electronic states (DOS) were performed for a model Al–Cu–Fe approximant for which the local and medium range orders mimic those in the icosahedral quasicrystal (Trambly de Laissardière and Fujiwara 1994) as well as for several crystalline phases related to quasicrystals (Trambly de Laisardière *et al* 1995a, Fournée *et al* 1998a).

Aluminium states being of rather extended character, one may expect that they are more sensitive to structural modifications than states of genuinely localized character such as d states. For instance, Fe and Cu d states distributions do not differ dramatically in crystals and quasicrystals as seen from soft x-ray spectroscopy (Belin *et al* 1992, Belin and Dankhazi 1993) and x-ray photoemission spectroscopy (Stadnik and Stroink 1993) measurements. Accordingly, analysis of extended-like states may point out fingerprints of the quasicrystalline atomic arrangement, if any, in comparison to crystalline structures closely related in composition as well as in local ordering. With this in mind, we have undertaken a systematic experimental investigation of Al electronic state distributions in a series of

crystalline Al–Cu–Fe (including fcc Al) as well as quasicrystalline alloys (samples are listed in table 1). To this end, we have used soft x-ray spectroscopy (SXS) techniques because they probe separately occupied and unoccupied DOS and are selective with respect to both the spectral symmetry and atomic site occupancy. We have also measured the Cu and Fe d states for a complete study of the occupied band. These measurements are compared to similar ones obtained from the icosahedral quasicrystal and its approximants, all of compositions found in the vicinity of $Al_6Cu_{2.5}Fe$ (in number of atoms).

After a qualitative discussion of the main features of the occupied Al 3s–d, Al 3p, Cu 3d and Fe 3d experimental densities of states (EDOS) in the various samples, the comparison between EDOSs is put on a more quantitative basis by computing the first moment of the normalized experimental distributions. It turns out from these data that the icosahedral compound corresponds to a sharp minimum of the contribution of Al 3p states to the compound cohesion energy whereas the mean of the other partial EDOSs remain constant over the same composition range. Meanwhile, from computation of the second moment of the Al 3p EDOS, it is observed that the orbital overlap of Al 3p states in this quasiperiodic intermetallic is more marked than in the nearby crystalline compounds. Al 3p states are responsible for the major part of the Hume-Rothery stability of these compounds since Al 3s states are repelled far from the Fermi energy. We conclude from these findings that quasicrystals are indeed essentially stabilized by the scattering of conduction states, as already emphasized by other authors but on quite a different and indirect experimental evidence (Biggs *et al* 1991, Klein *et al* 1991, Wang *et al* 1992, Pierce *et al* 1993). Equivalently, our data prove that the quasicrystal lies at a minimum of the free enthalpy of formation specifically due to this mechanism. To the best of our knowledge, this result is the first published so far that confirms on a direct experimental standpoint the electronic origin of the enhanced stability assigned to icosahedral order (Nelson and Spaepen 1989).

The paper is divided into five parts. After a summary of the experimental techniques used to obtain the partial EDOS, a subsection is devoted to the computation and physical meaning of the moments of order 1 and 2 of the density of states. Then comes a section on crystallographic data of the relevant samples and another about the characteristic features of the EDOS. The discussion section deals with a quantitative comparison of these measurements and focuses especially on partial Al 3p states since this gives the major contribution to the Hume-Rothery scattering mechanism.

2. Experiments

2.1. Samples

We have studied fcc Al (purity 99.99%) and a series of conventional crystalline phases as well as approximants and quasicrystalline Al–Cu–Fe phases as given in table 1. We have also compared the Al 3p distributions in a single-phase $Al_{70.5}Pd_{21}Mn_{8.5}$ sample, in three β-cubic CsCl phases and in two sets of samples of nominal compositions $Al_{62.8}Cu_{26}Fe_{11.2}$ and $Al_{61.8}Cu_{28}Fe_{10.4}$, respectively, which were both prepared either in the icosahedral state (after melt-spinning of the liquid alloy) or rhombohedral structure (by proper annealing). Preparation conditions of the various samples are not recalled here as they have already been reported elsewhere (Quiquandon *et al* 1996, Quivy *et al* 1996, Janot and Dubois 1998). These samples were prepared and fully characterized by x-ray and electron diffraction at CECM (Vitry, France) by Dr Y Calvayrac, at Ames Laboratory (Iowa, USA) by Dr D J Sordelet and by ourselves in Nancy.

Table 2. Name and x-ray transitions and probed electronic states; investigated energy ranges and monochromator used for the measurements.

Name of transition	Transition	Probed states	Energy range	Crystal or grating
Al Kβ	OB $\rightarrow$ Al 1s	Al 3p	1540–1565 eV	SiO_2 $10\bar{1}0$ $2d = 0.424$ nm
Al $L_{2,3}$	OB $\rightarrow$ Al $2p_{3/2}$	Al 3s–d	55–75 eV	grating 600 grooves mm^{-1}
Cu Lα	OB $\rightarrow$ Cu $2p_{3/2}$	Cu 3d–4s	910–940 eV	beryl $10\bar{1}0$ $2d = 1.582$ nm
Fe Lα	OB $\rightarrow$ Fe $2p_{3/2}$	Fe 3d–4s	700–715 eV	RbAp 001 $2d = 2.612$ nm

2.2. Soft x-ray and photoelectron spectroscopy measurements

The methodology applied in the present study uses soft x-ray spectroscopy experiments complemented by the measurement of the binding energy of various inner levels using x-ray photoelectron spectroscopy. The principles of the techniques and the experimental procedure have already been detailed in previous publications (see for example Belin-Ferré *et al* 1996a). We briefly recall them here. Soft x-ray emission spectroscopy (SXES) transitions involve an inner level of a solid and an outer level or the occupied band (OB). These transitions are governed by dipole selection rules ($\Delta l = \pm 1$ and $\Delta j = 0, \pm 1$) and therefore probe separately occupied s, p, d, ... states around each atomic site in the solid. The spectral distributions are proportional to the convolution product of the probed partial DOS by the energy distribution associated to the lifetime of the inner level involved in the x-ray transition. Therefore, no absolute DOS values are achieved from the measurements but it is possible to compare EDOS data for a given atom and chosen spectral character in various materials. According to the experimental conditions, the information may be spatially averaged over the bulk material (as for the present data) or may imply a significant contribution from the outmost layers at the surface of the solid.

Photoemission spectroscopy (PS) experiments measure the kinetic energies of electrons ejected from a solid following the interaction with an incident photon. Measurements are mainly surface sensitive depending on the electron mean free path in the material. The binding energy (BE) scale is often calibrated by taking the BE of the 1s level of contaminating carbon, always present at the surface of the sample, equal to 285.0 eV. The binding energy of electrons in the OB of a specimen are obtained all together, modulated by the relevant photoemission cross sections. These latter greatly favour d and f states (Yeh 1993) so that PS does not describe s and p OB states in our samples. However, using PS, the BE of core levels of a solid are obtained separately. Therefore, we can measure the BE of inner levels in our samples. This allowed us to set the Fermi level energy (E_F) on the x-ray transition energy scales of the spectral curves which we studied. Hence, this made it possible to adjust all EDOS in the same BE, thus supplying us with a complete picture of the OB distributions (Belin and Traverse 1991).

2.3. Experimental procedures

To describe the energy distributions of the occupied Al, Cu and Fe states we have investigated various x-ray transitions which are listed in table 2. The samples were water cooled and used as targets in the spectrometers. They were irradiated with incoming electrons with energy

sufficient to create the inner holes necessary for each transition to take place. The x-ray spectra were scanned with Johann type spectrometers fixed with a crystal bent under a radius of 50 cm or a grating bent under a radius of 1 m (table 2). The emitted photons were collected either with a gas flow proportional counter or a photocathode coupled with a channeltron. Emission spectra of pure fcc Al, Cu and Fe were measured as well for the sake of comparison and for energy calibration purposes. The final energy resolutions combine the intrinsic broadening due to the inner levels involved in the SXES processes and the instrumental function. They have been estimated to be of the order of 0.45 eV for Al Kβ, 0.35 eV for Al $L_{2,3}$ and 0.5 eV for both Cu and Fe spectra. The Al $2p_{3/2}$, Cu $2p_{3/2}$ and Fe $2p_{3/2}$ binding energies were achieved from PS measurements using the Mg Kα radiation (Mg $2p_{3/2} \rightarrow 1s$). The BE scale was calibrated as mentioned above with respect to the 1s level of contaminating C. The BE of the Al 1s level could not be measured directly. It was deduced from the energies of both the Al $2p_{3/2}$ level and the Al $2p_{3/2} \rightarrow 1s$ x-ray emission line. Hence, we could place E_F on the various Al, Cu and Fe x-ray transition energy scales within ± 0.1 eV for Al and ± 0.3 eV for the other elements.

2.4. Physical meaning and computation of the moments of order 1 and 2 of the EDOS

The contribution due to Al 3p states to the total binding energy is written

$$M_1 = -\int EN(E)\,\mathrm{d}E \Big/ \int N(E)\,\mathrm{d}E \tag{1}$$

with $N(E)$, the EDOS, namely:

$$N(E) \propto |\bar{M}|^2 n(E)^* V(E) \tag{2}$$

where $n(E)$ is the actual density of states which in x-ray spectroscopy experiments is convoluted by a Voigt function that results from the convolution of a Lorentzian function describing the core level finite lifetime and a Gaussian instrumental resolution function. $|\bar{M}|$ is the transition matrix element, which is usually taken to be constant or to only slowly vary with energy within the valence band. Hence, the moment of $N(E)$ calculated according to equation (1) is the same as the moment of $n(E)$ since all proportionality terms cancel and $|\bar{M}|$ is assumed to be independent of E. This holds true also for the moment of order 2 of $N(E)$ as given by equation (3) hereafter. A minus sign is inserted in the right-hand side of equation (1) so as to reconcile the spectroscopy energy data with thermodynamics (energies are quoted positive on the side of the valence band by convention in this paper). Similarly, the first moment of the other Al 3s–d partial EDOSs is calculated according to equation (1) by substituting the appropriate $N(E)$ data. The mean binding energy M_1 of Al 3p states represents only one among the many contributions to the total energy of the compound. We will show later that it is the only one that varies significantly within the composition field around the quasicrystal concentration. Furthermore, since Al 3s states are pushed far away from the Fermi level whereas d states are of localized character, this Al 3p partial EDOS represents by far the main contribution to the band term that Jones (1937, 1962) introduced in his interpretation of the peculiar stability of Hume-Rothery phases. The quantity in the denominator is used for normalization purposes so that the computed results normalize the band energy to one Al atom. On the other hand, in the tight binding theory the second moment of the partial DOS at site i is defined as the sum $\sum t_{ij}^2$ over all neighbours j, where t_{ij} is the hopping amplitude between sites i and j. It can be written as:

$$M_2 = \int E^2 N(E)\,\mathrm{d}E \Big/ \int N(E)\,\mathrm{d}E. \tag{3}$$

The higher the number of first neighbours is, the higher the second moment is because the number of channels from site i is increased. In the same respect, strong hybridization between

two neighbour sites will increase the second moment due to the large overlap of the contribution of each site to the total wavefunction. This effect can be detected when comparing two structures with shorter interatomic distances or higher hybridization according to the d metal involved in the structure.

3. Crystallographic background

Table 1 displays the unit cell parameters of θ-Al_2Cu, ϕ-$Al_{10}Cu_{10}Fe$ and ω-Al_7Cu_2Fe (see details of these structures in Fournée *et al* 1998b) as well as of rhombohedral, orthorhombic and 1/1 cubic Al–Cu–Fe approximants (Quiquandon *et al* 1995 and references therein, 1996, Quivy *et al* 1996). Pentagonal $Al_{63.6}Cu_{24.5}Fe_{11.9}$ corresponds to a periodic stacking of quasiperiodic planes with interplanar distance of 5.231 nm. All these alloys as well as the icosahedral Al–Cu–Fe compound itself are Hume-Rothery phases (Hume-Rothery 1926). Their electron to atom ratio (e/a) calculated from the usual values for the number of valence electrons per atom, namely three for Al, one for Cu and -2 for Fe, are given as well in table 1. We are also going to use data relevant to binary Al–Cu compounds which were investigated by Fournée *et al* (1998b). These crystals are typical Hume-Rothery compounds with e/a in the range 1.7 (δ-$Al_{35}Cu_{55}$) to 2.33 e^-/at (θ-Al_2Cu). Again, see Fournée *et al* (1998b) for details about the crystallography of these materials.

4. Spectroscopic data

4.1. Al electronic distributions

Figures 1(a) and 1(b) show the Al 3s–d and 3p EDOS curves in Al_7Cu_2Fe and Al_2Cu, respectively. For comparison purposes, we also display the same curves for fcc Al (figure 1(c)). The curves are normalized in the intensity scale between their own maxima and the baseline, linearly extrapolated from energy ranges where the variation of intensity is negligible. The results are described and discussed in the following sections.

4.1.1. Pure fcc Al. Data for fcc Al are reported in detail in many publications (Neddermayer 1973, 1974, Rooke 1968a, b, 1974) and have already been summarized in our previous papers (see, for example, Belin-Ferré *et al* 1996a, b). Let us briefly recall that both Al 3p and 3s–d EDOS curves overlap, emphasizing total hybridization over the whole OB extent. The inflexion point of the abrupt Al 3p emission arc tangent-like edge cuts E_F at half its maximum intensity; this is characteristic of a free-electron-like metal. Beyond the edge, towards increasing BE, there is a rounded maximum at about 1.3 eV and a parabolic decrease of intensity that is continued by a long monotonically decreasing tail. The edge of the Al 3s–d curve is even more abrupt. Note that it displays a sharp intense peak almost at E_F and then the shape is parabolic and exhibits also a long monotonically decreasing tail. This sharp peak is due to both the existence of states with a d-like character in a small energy range close to E_F (Léonard 1978, Papaconstantopoulos 1986) and to the generation of electron–hole pairs following the creation of the inner hole in a nearly free-electron system (Nozières and de Dominicis 1969).

4.1.2. Tetragonal ω-Al_7Cu_2Fe and θ-Al_2Cu The Al 3s–d and 3p EDOS curves in ω-Al_7Cu_2Fe and θ-Al_2Cu are shown in figures 1(a) and 1(b), respectively in comparison to fcc Al EDOS (figure 1(c)). The present data are free from any oxide contribution whereas previous measurements showed oxide contamination in an energy range of 5 to 9 eV from E_F (Trambly

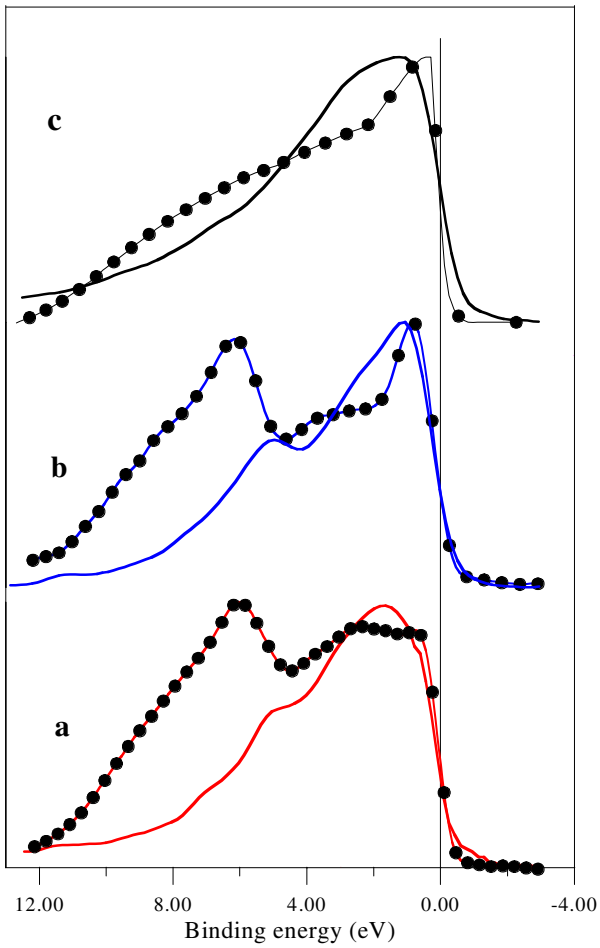

Figure 1. Al distribution curves in ω-Al_7Cu_2Fe (a), θ-Al_2Cu (b) and pure fcc Al (c): Al 3p curves are full lines whereas Al 3s–d curves are dotted curves, respectively.

de Laissardière *et al* 1995a). The shapes of the EDOS curves for the alloys differ from those in pure Al. In the direction of increasing binding energies below E_F, the Al 3s–d EDOSs (dotted curves in figure 1) show a marked peak in θ-Al_2Cu, followed by a bump, whereas such a peak is much less pronounced in ω-Al_7Cu_2Fe and merges into a bump of larger intensity than in θ-Al_2Cu. Both curves display a clear minimum around 4.0 eV and then a second maximum around 6 eV below E_F. The Al 3p EDOS also show a hollow around 4 eV and then their intensities decrease monotonically. We have shown that this relative minimum (antiresonance dip noted hereafter as AR dip) originates from a Fano-like interaction as described by Terakura (1977) between the extended Al states and the more localized Cu 3d states that lie in the middle of the OB (Trambly de Laissardière *et al* 1995a, Fournée *et al* 1998b) (figures 2(a) and 2(b)). Accordingly, the Al sub-bands are separated into two parts, located on each side of the Cu 3d states peak. In the two intermetallics, the Al 3s–d EDOS secondary maximum around 6 eV below E_F is in an energy range of decreasing intensity of the Al 3p EDOS, therefore the states in this energy range are almost s-like in character. In ω-Al_7Cu_2Fe, the Fe 3d spectral curve overlaps the Al curves, showing a mixing of the corresponding Al

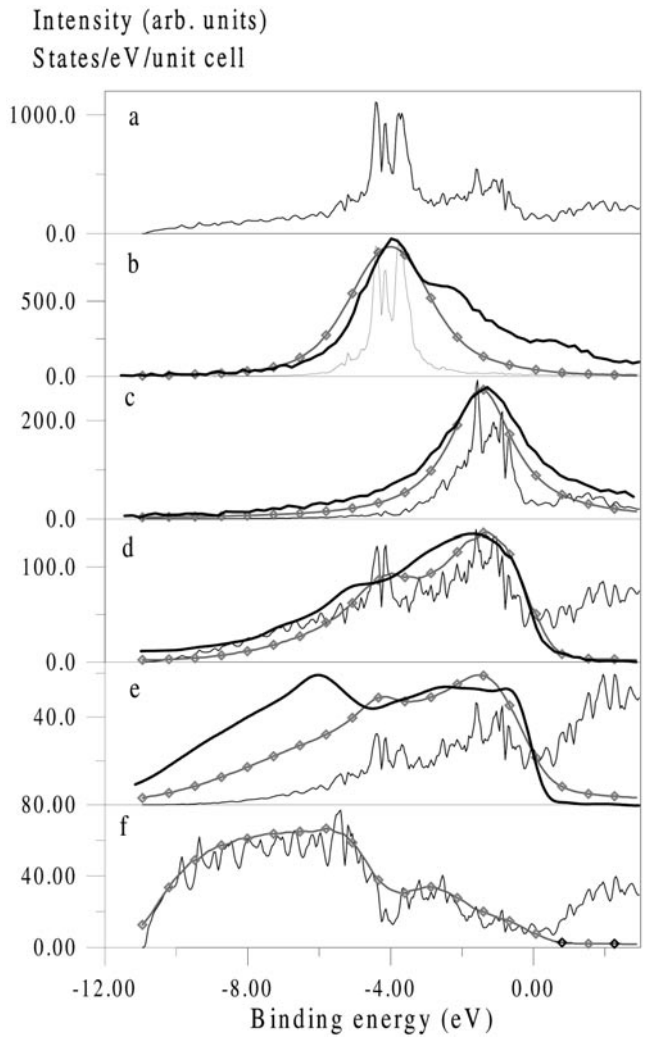

(a)

Figure 2. (a) Comparison between calculated (Trambly de Laissardière *et al* 1995a) and experimental DOS for ω-Al_7Cu_2Fe. The thick solid line represents the EDOS whereas the line with diamond symbols is for the calculated DOS broadened as explained in the text. The intensities are in arbitrary units. For completeness, the calculated DOS are also shown as thin solid lines with the intensity scale in states eV^{-1}/unit cell. Panel a is for the total calculated DOS. Panels b, c and d correspond to Cu d, Fe d and Al p OB states whereas panels e and f are for Al d and s OB states, respectively. (b) As in (a) but for θ-Al_2Cu. Here, panel a is for the total calculated DOS, whereas panels b, c, d and e correspond to Cu d, Al p, Al d and s OB states, respectively.

and Fe states near E_F (figure 2(a)).This is confirmed by partial DOS calculations of Trambly de Laissardière *et al* 1995a. Panels for Fe d and Al s, Al p and Al d states in figure 2(a) show that the Al and Fe calculated partial DOS curve (thin solid lines) retain the same shape within about 3 eV from E_F, thus emphasizing the mixing of the corresponding Fe and Al states. In both ω-Al_7Cu_2Fe and θ-Al_2Cu crystals, the intensity of the experimental Al 3p sub-band at E_F (thick solid line in figure 1) is slightly less than half its maximum and its edge is less steep than

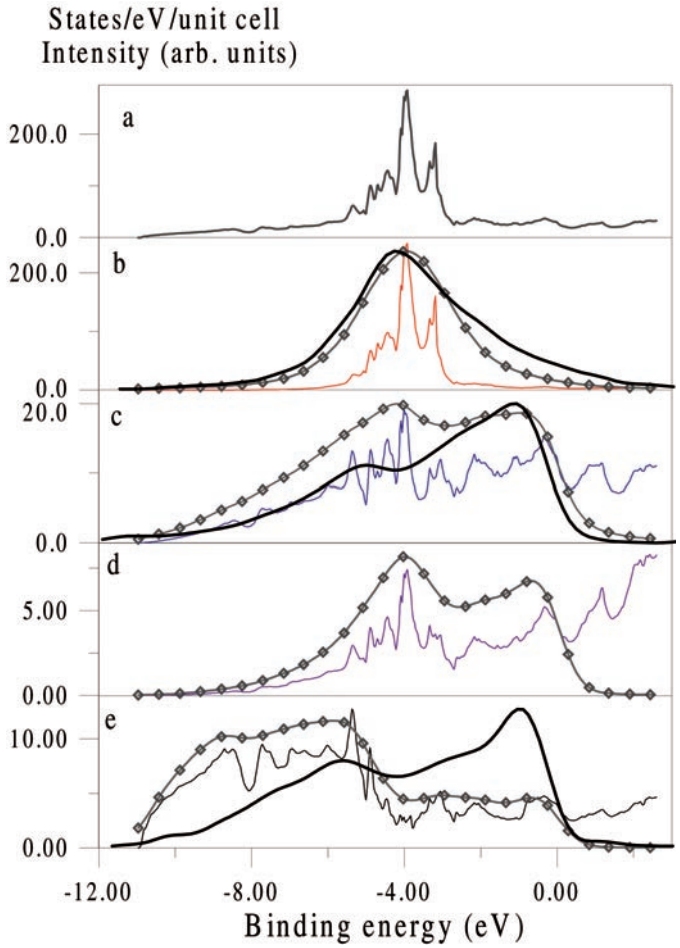

(b)

Figure 2. (Continued)

in fcc Al. The depletion of the Al states around E_F leads to the formation of a small pseudo-gap in agreement with the fact that these intermetallic crystals are of the Hume-Rothery type.

The energy positions and shapes of the different structures of the new Al 3s–d EDOS curves are in a much better agreement with the partial DOS calculations of Trambly de Laissardière *et al* (1995a) than our former data and confirm our previous interpretations as is shown in figures 2(a) and 2(b) for ω-Al_7Cu_2Fe and θ-Al_2Cu, respectively. These display the calculated partial DOS (thin solid lines), curves which result form the broadening of the calculated partial DOS to account for the life time of the core hole and the instrumental function (solid lines with diamonds) and the experimental curves (thick solid lines).

The experimental Al 3s–d curves which reflect both s and d spectral characters are compared only to the individual broadened 3s and 3d contributions with no further weight adjustment. Indeed, adding two fifths of the d DOS to the s DOS in order to better account for the experimental results (Goodings and Harris 1969) led to a good fit between calculation and experiment in the energy scale but differences remain in the intensity scales (Trambly de Laissardière *et al* 1995a, Fournée *et al* 1998a) hence we do not show the corresponding curves.

There are also discrepancies in the energy range of the AR dip where interaction with the Cu 3d states is present. This is seen in the bottom panels of figures 2(a) and 2(b) where the calculated partial DOS curves display sets of peaks in the AR dip range of the experimental curves. We have suggested that the calculated partial DOSs overestimate the p–d and d–d interactions between Al and Cu (Trambly de Laissardière *et al* 1995a). This point is still at the moment a matter of investigation (Papaconstantopoulos 1997). On the other hand, the calculations have stressed that the contribution of Al d-like states near E_F is significant in both alloys. Thus, a p–d-like character can be assigned to the Al states present close to E_F whereas they are s–p hybridized over about 6 eV from E_F and then more s-like in the high binding energy part of the OB.

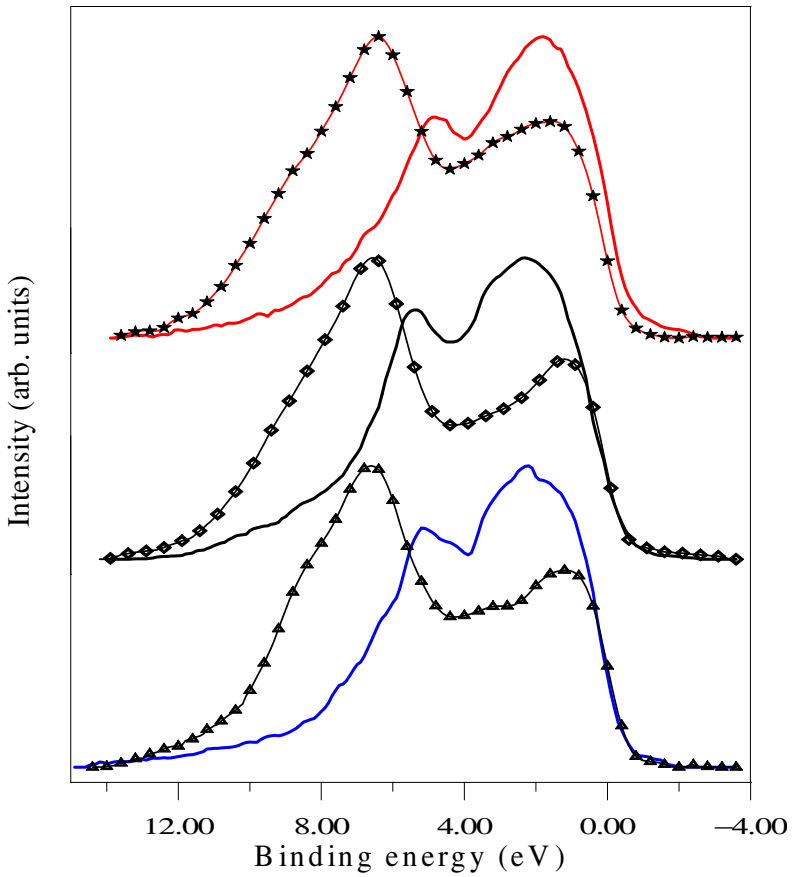

Figure 3. Experimental Al 3p (thick line) and Al 3s–d (thin line with symbols) for the β-cubic Al–Cu–Fe phases. Al content increases from bottom to top.

4.1.3. Cubic CsCl-type Al–Cu–Fe phases. The Al spectral curves for β-cubic $Al_{50}Cu_{35}Fe_{15}$, $Al_{46}Cu_{36}Fe_{18}$ and $Al_{55}Cu_{33}Fe_{12}$ phases of CsCl type are shown in figure 3. The shapes of the Al 3p and 3s–d are qualitatively the same. The intensities of the Al sub-bands close to E_F differ in these phases with respect to both ω-Al_7Cu_2Fe and θ-Al_2Cu alloys. However, the general organization of the OB partial contributions remains the same: almost pure s states lie at the bottom of the OB whereas states over about 6 eV from E_F are completely mixed. Note the significant AR dip around 4 eV below E_F in the Al 3p distributions. This is consistent with

a marked extended-like character of Al states in these intermetallics that therefore strongly interact with Cu d states. We will come back later to this point.

4.1.4. Icosahedral Al–Cu–Fe phase and its approximants. We have already discussed in previous papers the electronic interactions that take place in Al–Cu(Pd)–transition metal (TM) quasicrystals and related approximants. They are similar to those reported for the crystalline alloys with some differences in the amplitudes of the interactions (Belin *et al* 1992, Belin and Dankhazi 1993, Belin and Mayou 1993, Belin-Ferré *et al* 1996a). In all these alloys, due to the Fano-like mechanism as described by Terakura (1977), the OB Al sub-bands are also split in two distinct parts located on each side of the localized Cu d state maximum, and so there is an AR dip around 4 eV from E_F. There is also a mixing between Al states and TM d states in the close vicinity of E_F and a pronounced pseudo-gap at E_F (Belin *et al* 1992, Sadoc *et al* 1993b). Besides a Hume-Rothery mechanism (Friedel and Dénoyer 1987) and sp–d hybridization (Trambly de Laissardière *et al* 1995b) at E_F, structural effects can be invoked to interpret the formation of the pseudo-gap in the quasicrystalline phases (Belin-Ferré and Dubois 1996, Fournée *et al* 1998a).

In the Al 3p EDOS, we observe that the shoulder towards high BE of the AR dip (figure 4), is more marked in the crystalline approximants (three top curves) than in the icosahedral phase (bottom curve). The pentagonal phase (second curve from bottom in figure 4) looks more like the icosahedral quasicrystal than the other approximants, and indeed from the structural point of view it bears the most resemblance to the icosahedral phase (Gratias 1996). Thus, our observations suggest differences in OB Al 3p–Cu 3d interaction between the icosahedral Al–Cu–Fe quasicrystal and the approximants although there are similarities in the topological short range order of these alloys. By contrast, the Al 3s–d EDOSs are very similar for the icosahedral compound and its approximants (figure 5). However, for these distributions in the energy range close to E_F, the role of periodicity might be shadowed by the overlap of the s-like and d-like states. For these alloys, the ratio between the intensities of the maximum of the d-like peak close to E_F and the minimum of the AR dip around 4 eV from E_F is not strongly different from one sample to the other since it is 1.2 ± 0.10 for icosahedral Al–Cu–Fe and its pentagonal approximant and 1.3 ± 0.10 for the other approximants, respectively. Nevertheless, our data for Al 3p and 3s–d EDOSs suggest altogether that in the middle of the OB, Al states interact less strongly with Cu d states in the icosahedral quasicrystal than in the crystalline approximants. The Fano-like effect is stronger when extended states interact with localized states. In our samples, since the spectral character of Cu states is not modified, we deduce that Al states lose progressively their extended character when going from crystals to the icosahedral compound. Near to E_F, the Al s–d-like contribution to the OB is a little more intense in the icosahedral compound than in the crystalline alloys. Hence, we suppose that in the icosahedral compound there is a stronger mixing in this energy range between TM d states via the Al d-like counterpart as compared to that in the crystalline alloys.

The Al 3p pseudo-gap is characterized by the intensity I_{E_F} of the Al 3p curve at E_F and the distance δ to E_F taken at half the maximum intensity of the Al 3p sub-band. Remember that in pure fcc Al, in which by definition there is no pseudo-gap, these values are 0.5 and 0, respectively. The values of I_{E_F} and δ for the alloys of the present study are shown in figure 6. Remarkably, the Al 3p density of states at the Fermi energy reduces sharply in the vicinity of $e/a = 1.86\,\mathrm{e}^-/\mathrm{at}$ (figure 6(a)) and the pseudo-gap broadens abruptly (figure 6(b)) when going from rhombohedral, orthorhombic and pentagonal approximants to the perfect icosahedral quasicrystal. From approximants to the quasicrystalline phase, the strong interaction between the Al *d-like* and the Fe 3d states makes the Al states in the vicinity of E_F progressively of stronger localized-like character than in other compositionally related crystalline alloys such as

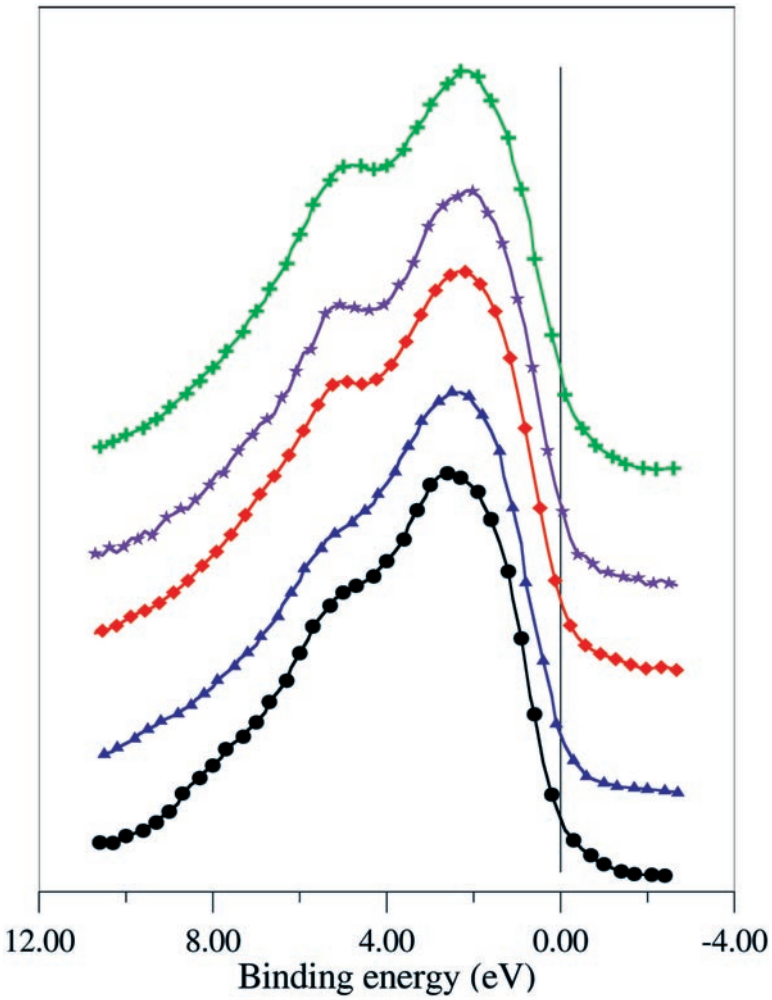

Figure 4. From bottom to top: Al 3p curves in icosahedral, pentagonal, rhombohedral and orthorhombic Al–Cu–Fe alloys and the 1/1 Al–Cu–Fe-Si cubic approximant.

the cubic intermetallics. Nevertheless, these cubic phases approach gradually the icosahedral compound as far as I_{E_F} and δ are considered (figure 6, solid line). This experimental feature confirms the assumption of Dong (1995) that these cubic phases are specific approximants of the icosahedral quasicrystal. Considering now regular Al–Cu–Fe crystals such as the Al–Cu Hume-Rothery compounds or the hexagonal ϕ-$Al_{10}Cu_{10}Fe$ and tetragonal ω-Al_7Cu_2Fe ternary crystals (figure 6, dashed line) proves the peculiar character of the quasicrystal regarding the depletion of the Al 3p EDOS at E_F. Hybridization between 3p and d states alone cannot be responsible for such an enhancement of the pseudo-gap in the quasicrystal as the comparison with the ternary crystals tells us. Hence, the Hume-Rothery mechanism is amplified in the icosahedral compound by structural scattering effects.

Finally, the whole of the SXES results show that over the full range of the occupied band, Al states in the quasicrystal are less extended-like in character than in the crystalline counterparts.

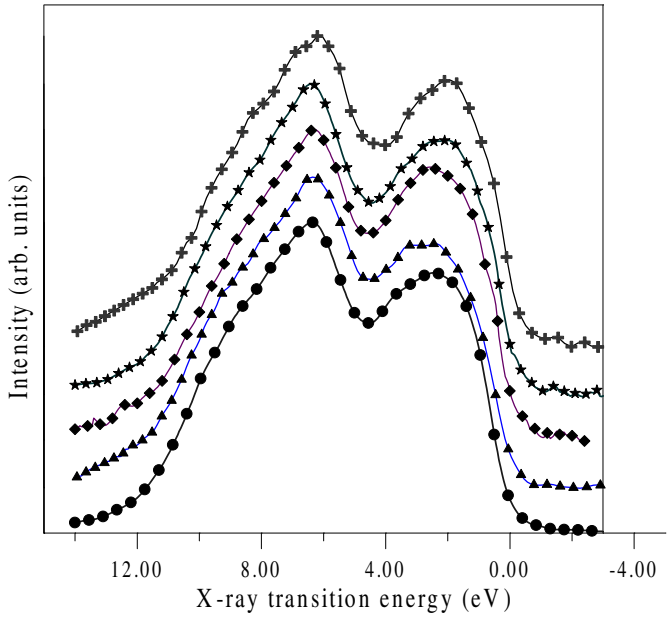

Figure 5. From bottom to top: Al 3s–d curves in icosahedral, pentagonal, rhombohedral and orthorhombic Al–Cu–Fe alloys and the 1/1 Al–Cu–Fe-Si cubic approximant.

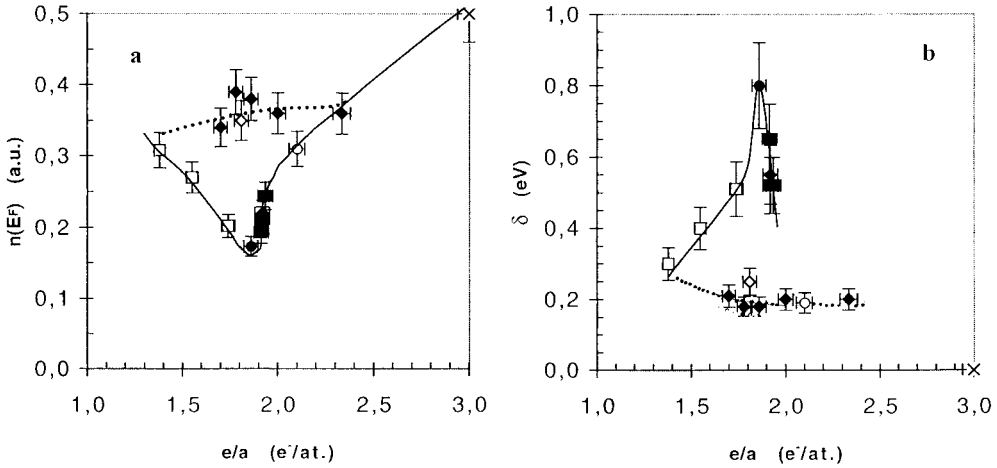

Figure 6. (a) Intensity at the Fermi energy of the Al 3p EDOS versus electron to atom ratio in fcc Al (cross), Al–Cu Hume-Rothery (solid diamonds), ϕ-$Al_{10}Cu_{10}Fe$ (open diamond), ω-Al_7Cu_2Fe (open circle), Al–Cu–Fe β-cubic CsCl-type phases (open squares), icosahedral (full circle), pentagonal, rhombohedral and orthorhombic (full squares) compounds. (b) As in (a) but for the width at half maximum δ of the Al 3p EDOS pseudo-gap. Lines are only guides for the eye.

4.1.5. Icosahedral versus rhombohedral compounds. The results discussed above correspond to approximant alloys of nominal compositions distinct from that of icosahedral $Al_{62}Cu_{25.5}Fe_{12.5}$. In order to ascertain the possible role of chemical composition, we have compared the Al 3p distributions in icosahedral and rhombohedral samples of identical nominal compositions. This comparison was achieved thanks to two sets of samples with

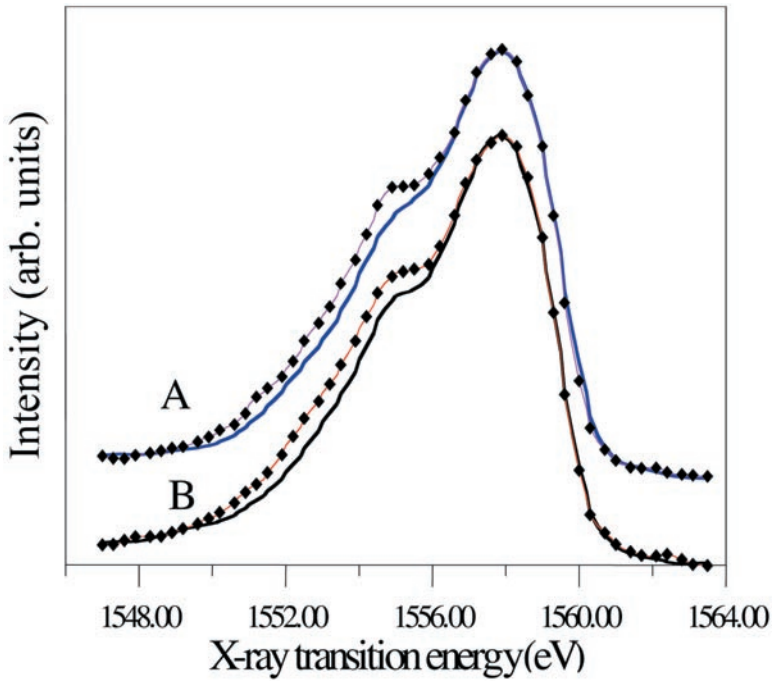

Figure 7. Al 3p distribution curves in $Al_{61.6}Cu_{28}Fe_{10.4}$ (A) and $Al_{62.8}Cu_{26}Fe_{11.2}$ (B). The full lines correspond to the icosahedral compounds and the curves with diamonds to the rhombohedral phases.

distinct compositions, namely $Al_{62.8}Cu_{26}Fe_{11.2}$ and $Al_{61.6}Cu_{28}Fe_{10.4}$. For each composition, the icosahedral structure was obtained in the as-cast state, hence in a metastable state, whereas proper annealing led to the stable rhombohedral crystals. The corresponding curves are plotted in figure 7 in the x-ray transition energy scale. The shoulders present around 1555 eV are significantly less marked for the icosahedral phases than for their rhombohedral counterparts. The difference between the two EDOSs in each set of data is clearly above experimental resolution and implies a significant contrast between rhombohedral and icosahedral samples. The more marked the shoulder, the more intense the interaction between Cu 3d and Al 3p states which is therefore more important in the stable rhombohedral compound than in the icosahedral sample of identical composition. The origin of this effect might be related to the Cu neighbourhood of the Al sites (i.e. more Cu neighbours and/or shorter Al–Cu distances), which is not yet known from a complete crystallographic analysis of these structures. Artefacts due to the preparation by rapid solidification of the icosahedral samples, which induces a high phason strain level, may also play a role. The influence of an intrinsically more localized character of the Al 3p states in icosahedral compounds may be involved as well (see section 4.4) since their interaction with Cu 3d states is then less marked (Terakura 1977).

4.2. Cu electronic distributions

Partial DOS calculations performed for crystalline Al_2Cu, Cu_3Al, Al_7Cu_2Fe and quasicrystalline approximants show that the Cu d states are dominant in all alloys. They are found at about 4 eV below E_F, i.e. approximately 1 eV lower than in pure Cu. The width of the Cu d band in all the samples we have studied is reduced as compared to that of pure Cu.

Band narrowing is a consequence of both the decrease of the d–d hopping amplitudes and the number of possible hopping channels, i.e. the Cu d-band width reduction is connected to the coordination of the Cu atoms in the alloy. To exemplify, we have computed the band width in Al_2Cu of fluorite type where a Cu atom is at the centre of a first shell occupied only by eight Al atoms at 0.26 nm, 12 other Cu atoms being located on a second shell at 0.42 nm. This band width is contracted by 0.5 eV in comparison to that calculated for metallic copper where a Cu atom is surrounded by 12 Cu atoms at a distance of 0.255 nm. Furthermore, the position of the d band is determined by its interaction with the Al band. Actually, we have shown that the shift of the d band towards the high binding energies is sensitive to the Cu–Al coordination number and distance. Here, according to our experimental accuracy, the Cu maximum does not differ significantly from one sample to the other. As to the band width, it is 2.6 ± 0.1 eV for pure Cu, 2.4 ± 0.1 eV for Al_2Cu, 2.2 ± 0.1 eV for Al_7Cu_2Fe, 2.1 ± 0.1 eV, 2.3 ± 0.1 eV and 2.5 ± 0.1 eV for the pentagonal, orthorhombic and 1/1 cubic approximants, respectively, and 2.0 ± 0.1 eV for the icosahedral compound. This confirms that the Cu coordination and Al–Cu distances should be similar in the icosahedral and pentagonal phases. They should slightly differ in the orthorhombic approximant and Al_7Cu_2Fe and vary more significantly in the cubic 1/1 alloy (Fournée *et al* 1998a).

4.3. Fe electronic distributions

The interaction between Al and Fe states in the alloys tends to fill the Fe 3d occupied sub-band and thus to shift the Fe 3d band towards E_F with respect to the pure metal. We have found that the Fe 3d band states maximum is at 2.3 ± 0.3 eV from EF in the pure metal and 1.6 ± 0.3 eV from E_F in crystalline Al_7Cu_2Fe whereas it is at 1.3 ± 0.3 eV from E_F in the icosahedral compound. Systematic verification for all the samples studied here would have required to very carefully determine the binding energy of the Fe core level involved in each Fe 3d SXES measurement. We have restricted ourselves to a few cases since such a determination is rather difficult with satisfactory accuracy due to the low Fe concentration in the samples. Another possibility to ascertain the charge transfer would be to investigate the energy distribution of the Fe d unoccupied states. Indeed, changes in the shapes are expected when filling the occupied d-like band. This is what we have observed when going from pure Fe to Al_7Cu_2Fe and to the icosahedral quasicrystal (Sadoc *et al* 1993b, Belin and Mayou 1993).

4.4. Moments of order 1 and 2 of the Al distributions

Calculation of the first moment M_1 of the Al 3p and Al 3s–d experimental distributions has been made for the series of β-cubic Al–Cu–Fe phases, approximants and perfect quasicrystal mentioned above and also for several Al–Cu Hume-Rothery alloys. Figure 8(a) shows the plot of M_1 for the Al 3p EDOS against the e/a ratio. It clearly presents a minimum for the icosahedral $Al_{62}Cu_{25.5}Fe_{12.5}$ compound which corresponds to $e/a = 1.86$ e^-/at. The value of M_1 for the Al 3s–d EDOS (figure 8(b)) displays a less marked minimum at the same value of e/a whereas calculations for the Cu 3d and Fe 3d EDOS distributions show that they are mostly insensitive to the variation of the electron concentration. The existence of the minimum of M1 for both Al 3p and 3s–d EDOS at the position of the icosahedral compound coincides with calorimetric investigations from which it was concluded that the icosahedral structure may form the ground state in this region of the Al–Cu–Fe phase diagram (Saadi *et al* 1995). Accordingly, our data show unambiguously that the major contribution to the stability of the icosahedral compound arises from Hume-Rothery scattering of nearly free Al 3p states (and to a lesser extent Al 3s states). To the best of our knowledge, this is the first direct evidence

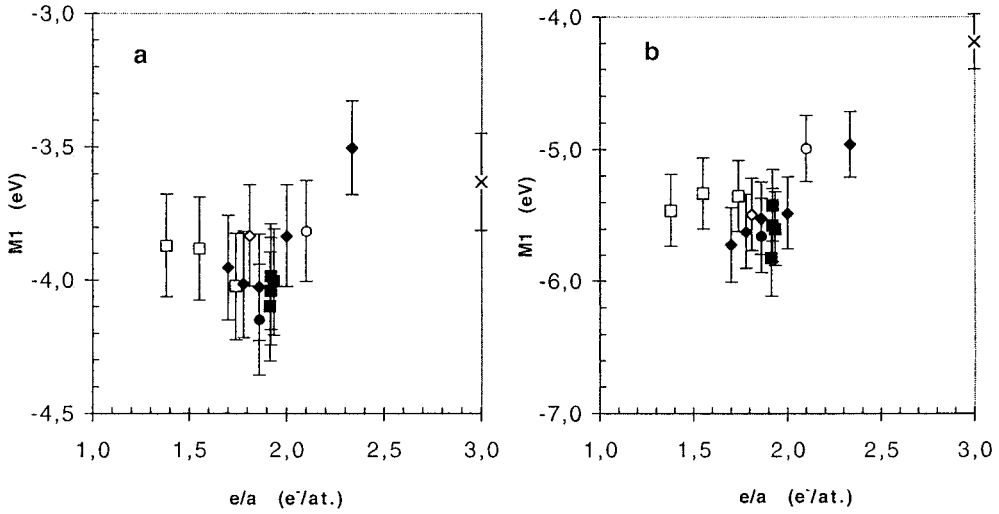

Figure 8. Moment of order 1 of the Al 3p distribution versus electron to atom ratio in fcc Al (cross), Al–Cu Hume-Rothery (solid diamonds), ϕ-$Al_{10}Cu_{10}Fe$ (open diamond), ω-Al_7Cu_2Fe (open circle), Al–Cu–Fe β-cubic CsCl-type phases (open squares), icosahedral (full circle), pentagonal, rhombohedral and orthorhombic (full squares) compounds. (b) As in (a) but for the Al 3s–d EDOS.

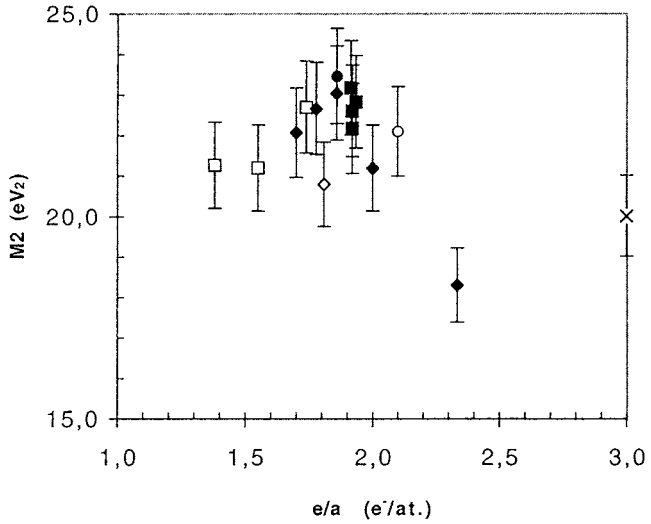

Figure 9. Moment of order 2 of the Al 3p distribution versus electron to atom ratio e/a in fcc Al (cross), Al–Cu Hume-Rothery (solid diamonds), ϕ-$Al_{10}Cu_{10}Fe$ (open diamond), ω-Al_7Cu_2Fe (open circle), Al–Cu–Fe β-cubic CsCl-type phases (open squares), icosahedral (full circle), pentagonal, rhombohedral and orthorhombic (full squares) compounds.

supplied so far to demonstrate that the specific stability of icosahedral quasicrystals is related to the Al 3p EDOS in Al-based intermetallics.

The moment of order 2, M_2, was calculated from the experimental electronic distributions for the same set of samples (figure 9). As a matter of fact, there is a marked maximum for the icosahedral $Al_{62}Cu_{25.5}Fe_{12.5}$ compound with $e/a = 1.86$ e^-/at. As explained in

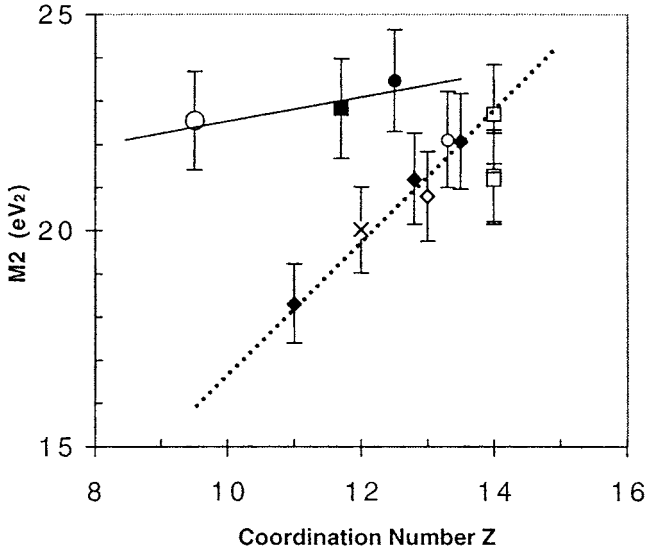

Figure 10. Moment of order 2 of the Al 3p distribution versus coordination number Z in fcc Al (cross), Al–Cu Hume-Rothery (solid diamonds), ϕ-$Al_{10}Cu_{10}Fe$ (open diamond), ω-Al_7Cu_2Fe (open circle), Al–Cu–Fe β-cubic CsCl-type phases (open squares), icosahedral (full circle), pentagonal, rhombohedral and orthorhombic (full squares) compounds. The large open cirlce refers to icosahedral $Al_{70.5}Pd_{21}Mn_{8.5}$.

section 2.4, one expects that M_2 varies with the number Z of neighbours as displayed in figure 10. For completeness, we have also shown the M_2 value for icosahedral Al–Pd–Mn. This linear correlation is actually observed for the Hume-Rothery alloys where M_2 is the highest for the largest Cu content. This is also noticed with the β-phases for which M_2 slightly increases with decreasing Fe content. We assign this tendency to super-structure ordering effects in these peculiar phases (Dong and Dubois 1993, Dong 1995). For the icosahedral samples, the Z values were taken from EXAFS measurements (Sadoc *et al* 1991, Sadoc and Dubois 1992) and from a calculation on the real structure for the 1/1 cubic approximant Al–Cu–Fe–Si determined according to the Rietveld method (Yamada *et al* 1999). Atomic positions are not known yet for the other approximants. Similarly to the crystalline alloys, the linear M_2 versus Z correlation is followed by the icosahedral Al–Cu–Fe and Al–Pd–Mn quasicrystals and the cubic 1/1 approximant but at higher values of M_2. We interpret this difference with respect to regular crystals as pointing out a stronger hybridization between Al 3p and Fe 3d states in these alloys as compared to the conventional crystals. Altogether, these observations confirm the interplay between the Hume-Rothery scattering stabilization mechanism and s–p–d hybridisation at E_F in quasicrystals and explain the enhanced stability of the icosahedral $Al_{62}Cu_{25.5}Fe_{12.5}$ quasicrystal.

5. Conclusion

We have used the soft x-ray emission spectroscopy technique to investigate partial Al occupied state distributions in icosahedral $Al_{62}Cu_{25.5}Fe_{12.5}$ and in a series of both approximants and conventional crystalline alloys. Comparison between experiments and calculations for tetragonal Al_2Cu and Al_7Cu_2Fe shows good agreement, thus giving confidence in the relevance of the SXES results. From the various features of the spectra of the $Al_{62}Cu_{25.5}Fe_{12.5}$ icosahedral

compound and its crystalline approximants, we conclude that the Al–Cu interaction is less marked and Al–Fe interaction is stronger in the icosahedral compound than in the related crystalline phases. This indicates that Al occupied states are more localized in the atomic icosahedral arrangement than in the periodic counterparts. From the variation with the electron density and coordination number of the first and second moments of the Al 3p distribution, we have supplied direct evidence that the stability of the icosahedral state results from an interplay between Hume-Rothery scattering effects and s–p–d hybridization at the Fermi energy E_F.

Acknowledgments

We are most grateful to Dr D A Papaconstantopoulos for a critical reading of the manuscript. We thank Dr D Gratias, Dr D Mayou and Dr M Quiquandon for stimulating discussions and Dr Y Calvayrac and Dr D J Sordelet for the provision of approximant and cubic phase samples. This work was supported in part by the Austrian Ministry of Research, East West Co-operation programme, under the title 'Soft x-ray emission spectroscopy of metallic systems'.

References

Audier M and Guyot P 1989 *Quasicrystals and Incommensurate Structures in Condensed Matter* ed M J Yacaman and D Romeu (Singapore: World Scientific) p 288
Belin E and Dankhazi Z 1993 *J. Non-Cryst. Solids* **153–154** 298
Belin E, Dankhazi Z, Sadoc A, Calvayrac Y, Klein T and Dubois J M 1992 *J. Phys.: Condens. Matter* **4** 4459
Belin E and Mayou D 1993 *Phys. Scr.* **49** 356
Belin E and Traverse A 1991 *J. Phys.: Condens. Matter* **3** 2157
Belin-Ferré E, Dankhazi Z, Sadoc A, Berger C, Müller H and Kirchmayr H 1996a *J. Phys.: Condens. Matter* **8** 3513
Belin-Ferré E and Dubois J M 1996 *J. Phys.: Condens. Matter* **8** L717
Belin-Ferré E, Fournée V and Dubois J M 1996b *New Horizons in Quasicrystals: Research and Applications* ed A I Goldman (Singapore: World Scientific) p 9
Berger C 1994 *Lectures on Quasicrystals* ed F Hippert and D Gratias (Les Ulis: Editions de Physique) p 463
Berger C, Gignoux C, Tjernberg O, Lindqvist P, Cyrot-Lackmann F and Calvayrac Y 1995 *Physica* B **204** 44
Biggs B D, Li Y and Poon S J 1991 *Phys. Rev.* B **43** 8747
Calvayrac Y, Quivy A, Bessière M, Lefèbvre S, Cornier-Quiquandon M and Gratias D 1990 *J. Physique* **51** 417
Dong C 1995 *J. Physique* **5** 1625
Dong C and Dubois J M 1993 *J. Non-Cryst. Solids* **159** 107
Fournée V, Belin-Ferré E and Dubois J M 1998b *J. Phys.: Condens. Matter* **10** 4231
Fournée V, Mazin I, Papaconstantopoulos D A and Belin-Ferré E 1998a *Phil. Mag.* B **79** 205
Friedel J and Denoyer F 1987 *C. R. Acad. Sci., Paris* B **305** 171
Goodings D A and Harris R 1969 *J. Phys. C: Solid State Phys.* **2** 1808
Gratias D 1996 private communication
Gratias D, Calvayrac Y, Devaud-Rzepski J, Faudot F, Harmelin M, Quivy A and Bancel P 1993 *J. Non-Cryst. Solids* **153–154** 482
Goodings D A and Harris R 1969 *J. Phys. C: Solid State Phys.* **2** 1808
Hippert F 1997 private communication
Hippert F, Brand R A, Pelloth J and Calvayrac Y 1995 *Quasicrystals* ed C Janot and R Mosseri (Singapore: World Scientific) p 464
Hume-Rothery W 1926 *J. Int. Metals* **35** 295
Janot C and Dubois J M 1998 *Les Quasicristaux, Matière à Paradoxes* (Les Ulis: Editions de Physique)
Jones H 1937 *Proc. Phys. Soc.* **49** 250
——1962 *J. Physique Radium* **23** 637
Kang S S, Malaman B, Venturini G and Dubois J M 1992 *Acta Crystallogr.* B **48** 770
Klein T, Berger C, Mayou D and Cyrot-Lackmann F 1991 *Phys. Rev. Lett.* **66** 2907
Léonard P 1978 *J. Phys. F: Met. Phys.* **8** 467
Neddermayer H 1973 *Band Structure Spectroscopy of Metals and Alloys* ed D J Fabian and L M Watson (London: Academic) p 153 and references therein
Neddermayer H 1974 *Z. Phys* **271** 329

Nelson D R and Spaepen F 1989 *Solid State Phys.* **42** 1
Nozières P and de Dominicis C T 1969 *Phys. Rev.* **178** 6105
Papaconstantopoulos D A 1986 *Handbook of the Band Structures of Elemental Solids* (New York: Plenum) p 208
——1997 private communication
Pierce F S, Bancel P A, Biggs B D, Guo Q and Poon S J 1993 *Phys. Rev.* B **47** 5670
Quiquandon M, Calvayrac Y, Quivy A, Faudot F and Gratias D 1999 *Quasicrystals (Mater. Res. Soc. Symp. Proc. 553)* ed J M Dubois *et al* (Warrendale, PA: Material Research Society) p 95
Quiquandon M, Quivy A, Devaud J, Faudot F, Lefèbvre S, Bessière M and Calvayrac Y 1996 *J. Phys.: Condens. Matter* **8** 2487
Quiquandon M, Quivy A, Faudot F, Saadi N, Calvayrac Y, Lefèbvre S and Bessière M 1995 *Quasicrystals* ed C Janot and R Mosseri (Singapore: World Scientific) p 152
Quivy A, Quiquandon M, Calvayrac Y, Faudot F, Gratias D, Berger C, Brand R A, Simonet V and Hippert F 1996 *J. Phys.: Condens. Matter* **8** 4223
Rooke G A 1968a *J. Phys. C: Solid State Phys.* **1** 767
Rooke G A 1968b *J. Phys. C: Solid State Phys.* **1** 776
Rooke G A 1974 *X-ray Spectroscopy* ed L V Azaroff (New York: McGraw-Hill)
Saadi N, Faudot F, Gratias D and Legendre B 1995 *Quasicrystals* ed C Janot and R Mosseri (Singapore: World Scientific) p 656
Sadoc A, Berger C and Calvayrac Y 1993a *Phil. Mag.* B **68** 475
Sadoc A, Belin E, Dankhazi Z and Flank A M 1993b *J. Non-Cryst. Solids* **153–154** 338
Sadoc A and Dubois J M 1992 *Phil. Mag.* B **66** 541
Sadoc A, Flank A M and Lagarde P 1991 *X-ray Absorption Fine Structure* ed S Strasman (New York: Ellis Horwood)
Stadnik Z M and Stroink G 1993 *Phys. Rev.* B **47** 100
Sugiyama K, Kaji N, Yubuta K, Hiraga K and Ishimasa T 1998 *Quasicrystals* ed S Takeuchi and T Fujiwara (Singapore: World Scientific) p 199
Terakura K 1977 *J. Phys. F: Met. Phys.* **7** 1773
Trambly de Laissardière G, Dankhazi Z, Belin E, Sadoc A, Nguyen Manh D, Mayou D, Papaconstantopoulos D A and Keegan M A 1995a *Phys. Rev.* B **51** 14035
Trambly de Laissardière G and Fujiwara T 1994 *Phys. Rev.* B **50** 5999
Trambly de Laissardière G, Nguyen Manh D, Magaud L, Julien J P, Cyrot-Lackmann F and Mayou D 1995b *Phys. Rev.* B **52** 7920
Wang K, Scheidt C, Garoche P and Calvayrac Y 1992 *J. Physique* **2** 1553
Yamada H, Takeuchi T and Mizutani U 1999 *Quasicrystals (Mater. Res. Soc. Symp. Proc. 553)* ed J M Dubois (Warrendale, PA: Material Research Society) p 117
Yeh J 1993 *Atomic Calculation of Photoionization Cross sections and Asymmetry Parameters* (New York: Gordon and Breach)